HADLEY CENTRE TECHNICAL NOTE NO. 4

CHARACTERISING GCM LAND SURFACE SCHEMES TO UNDERSTAND THEIR RESPONSES TO CLIMATE CHANGE.

by

N.Gedney, P.M. Cox, H. Douville, J Polcher, P.J.Valdes

Submitted to Journal of Climate

January 1999

Hadley Centre for Climate Prediction and Research
Meteorological Office
London Road
Bracknell
Berkshire RG12 2SY

Characterising GCM land surface schemes to understand their responses to climate change

[1]N. Gedney, [1]P.M. Cox
[2]H. Douville, [3]J. Polcher, [4]P. J. Valdes

[1]Hadley Centre, Met Office, Bracknell, Berks RG12 2SY, UK
[2]Meteo-France, Toulouse, France
[3]Laboratoire de Meteorologie Dynamique du CNRS, Gif-sur-Yvette, France
[4]Reading University, Reading, U.K.

December 22, 1998

Abstract

The impact of land surface representation on GCM simulations of climate change is analysed using 8 climate change experiments, carried out with 4 GCMs each utilising 2 different land surface schemes (LSSs). In the regions studied (Amazonia, the Sahel and Southern Europe) the simulations differ markedly in terms of their predicted changes in evapotranspiration and soil moisture. This is only partly as a result of differences in the predicted changes in precipitation and available energy. A simple "bucket model" characterisation of each LSS, demonstrates that the different hydrological sensitivities are also strongly dependent on properties of the LSS; most notably the runoff which occurs when evaporation is marginally soil moisture limited. This parameter, "Y_c", varies significantly amongst the LSSs, and significantly influences both the soil moisture in the $1\times CO_2$ control climate, and the sensitivity of both evaporation and soil moisture to climate change. It is concluded that uncertainty in the predicted changes in surface hydrology are more dependent on such gross features of the runoff versus soil moisture curve, than on the detailed treatment of evapotranspiration.

1 Introduction

Land surface modelling is cited as one of the major causes of the uncertainties in current climate change predictions (Houghton *et al* (1995)). This is especially significant given the need to assess many of the the impacts of climatic change, such as the effect on agriculture and changes in the occurrence of extreme hydrological events like drought and flooding.

Some climate simulations suggest that there will be an increased likelihood of summer drought in midlatitudes in an enhanced greenhouse gas climate (Gregory *et al* (1997)). Successful assessment of its potential severity is dependent on adequate modelling of the land surface. However PILPS (Henderson-Sellers *et al* (1996)) demonstrates that there is a wide disparity between GCM land surface schemes (LSSs), with little agreement on the modelled soil moisture and evaporation.

Koster and Milly (1997) analysed part of the PILPS 2a experiment where identical atmospheric conditions were used to force a number of LSSs offline, which in principle have identically prescribed vegetation and soil characteristics. They showed that the hydrological behaviour of the LSSs is fundamentally dependent on the interplay between evaporation and runoff, and that it was possible to understand the differences in terms of a few simple effective characteristics which can be associated with the monthly mean water balance of each LSS.

We use a similar methodology to assess the role of LSSs in predicted changes in surface hydrology as a result of climate change. This is carried out with a number of experiments using different GCMs and LSSs (described in section 2). Firstly, the behaviour of each LSS is characterised in the $1\times CO_2$ simulations over three specific regions: Amazonia, the Sahel and Southern Europe. This is achieved by examining the sensitivity of the partitioning between runoff and evapotranspiration to soil moisture for each LSS. We show that this can be used to understand the regionally averaged annual mean soil moisture of each LSS in the $1\times CO_2$ control runs (section 3).

This characterisation can then be used to estimate and explain the LSS response to the change in climate forcing, as defined by changes in precipitation and available energy. The methodology for this is described in section 3b and is applied to Amazonia, the Sahel and Southern Europe in section 4.

Section 5 summarises the findings in terms of a generic non-linear bucket model, which is used to separate the respective influences of the control climate and the LSS characteristics on the hydrological sensitivity.

2 Experiment

Four groups participated in the GCM experiments: the Hadley Centre, the Laboratoire de Meteorologie Dynamique du CNRS (LMD), Meteo-France (CNRM) and the University of Reading. Each performed two time-slice experiments, both consisting of a $1\times CO_2$ and $2\times CO_2$ run. The AMIP (Gates (1992)) sea surface temperature and sea-ice fields were used in the $1\times CO_2$ experiment. The temperature and sea-ice changes produced by the Hadley Centre transient climate change run (Mitchell *et al* (1995)) were applied to the AMIP climatological fields to produce the boundary conditions for the $2\times CO_2$ time-slice simulations. All simulations were at least ten years long after an initial spinup period. Each experiment pair were implemented with two different LSSs coupled to an otherwise identical GCM. The differences between each LSS pair were not controlled, but they turned out to be mainly associated with surface hydrology (see Table 1). Two of the groups (the Hadley Centre and CNRM) included the effects of CO_2 induced stomatal closure in one of their $2\times CO_2$ runs (Hb and Cb respectively). In fact, this was the only difference between Ca and Cb, hence the control runs for Ca and Cb are identical. There is a number of other LSS specific points worth noting; Lb uses a bucket-type soil hydrology and does not explicitly parameterise stomatal resistance. Runoff only occurs in La and Lb when the soil is saturated, making these models very sensitive to temporal rainfall patterns. In La there is no simple relationship between rootzone soil moisture and evapotranspiration, because vegetation becomes unstressed if the movable top layer of soil becomes saturated, even if the rootzone as a whole is moisture deficient.

The three regions analysed are: Amazonia, the Sahel and Southern Europe, (see table 2).

3 Characterising the land surface schemes

Following the methodology of Koster and Milly (1997), a bucket type formulation is utilised to model how the suite of LSSs respond to limited soil moisture under snow free conditions and ignoring interception, E_i. However, the potential evaporation rate, E_p, was not available from all of the GCM experiments, so we replaced E_p in the usual bucket formulation with effective available energy, A_e:

$$A_e = \frac{R_N - G - LE_i}{L} \tag{1}$$

Here A_e has been scaled to have the units of a water flux, and R_N, G and L are the net radiation, the ground heat flux and the latent heat of vaporisation. In this model, evapotranspiration (i.e. bare soil evaporation plus transpiration), E_e, is therefore assumed to be dependent on the effective available energy, A_e, and the rootzone soil moisture, M, through a soil moisture stress factor, β:

$$E_e = \beta\, A_e \tag{2}$$

It is also convenient to scale the soil moisture by its active range, which is defined as the point at which evapotranspiration starts (M_{wilt}) to the point beyond which evapotranspiration is not constrained by soil moisture (M_{crit}):

$$\mu = \frac{M - M_{wilt}}{M_{crit} - M_{wilt}} \tag{3}$$

The critical and wilting points were estimated from the regionally averaged values of the parameters in each LSS. In terms of this scaled variable, β takes the simple piecewise linear dependence:

$$\beta(\mu) = \begin{cases} \beta_c\,\mu & \text{for } \mu \le 1 \\ \beta_c & \text{for } \mu > 1 \end{cases} \tag{4}$$

where β_c is the evaporative fraction at the critical soil moisture concentration. In the original bucket formulation (Manabe (1969)) $\beta_c = 1$, but this assumption is not generally valid for more complex LSSs which include a finite stomatal resistance even in times of plentiful water supply.

Assuming that drainage dominates over surface runoff, the total runoff, Y, is likely to be most dependent on deep soil moisture, but for simplicity it is assumed that rootzone soil moisture provides a good surrogate variable (i.e. that changes in the soil moisture vertical profile are insignificant). Runoff is taken to vary with a power, c, of the scaled soil moisture, which is inline with the Clapp and Hornberger (1978) curves used in many LSSs and is sufficiently general to fit the runoff from most other models:

$$Y = Y_c \mu^c \tag{5}$$

Figures 1a and 1b show the variation of β and Y with μ, for the Amazonian region, as diagnosed using monthly means from each of the $1\times CO_2$ simulations. There are a number of things to notice about these curves. Firstly, there is a definite tendency for the gradient of β with respect to μ to be significant for $\mu < 1$ and small for $\mu > 1$, in general agreement with equation 4. Soil moisture heterogeneity across the region acts to smooth any such underlying β curve (Entekhabi and Eagleson (1989)), but the piecewise linear form still appears to provide a good qualitative description. The second thing to note, is that the runoff curves from the various models differ markedly, with some models producing negligible runoff at the critical point (e.g. Ha, Hb) and others producing significant runoff even at much lower soil moistures (e.g. Ua, Ub, La , Lb). In general the models give runoff values which increase monotonically with soil moisture, but there is also some evidence of hysteresis in the $Y - \mu$ curve. Finally, it is clear that the models tend to occupy quite distinct μ-regimes, with some models rarely experiencing moisture stress (e.g. Ha, Hb) and others remaining moisture stressed throughout the year (e.g. Ua, Ub, La, Lb). Much of this paper is devoted to analysing the reasons for these disparate hydrological regimes, in terms of the respective impacts of differences amongst the climate forcings and the LSSs.

However, for now, the relatively small range of μ experienced by each LSS provides a further simplification. We can linearly expand about the annual mean soil moisture of the control state, $\bar{\mu}$:

$$\beta(\mu) = \beta(\bar{\mu}) + \beta'(\mu - \bar{\mu}) \tag{6}$$

$$Y(\mu) = Y(\bar{\mu}) + Y'(\mu - \bar{\mu}) \tag{7}$$

where β' and Y' are the gradients of β and Y with respect to μ at $\mu = \bar{\mu}$. In order to separate the control state ($\bar{\mu}$) from the underlying properties of the surface scheme we recast equations 6 and 7 in the form:

$$\beta(\mu) = \beta_c + \beta'(\mu - 1) \tag{8}$$

$$Y(\mu) = Y_c + Y'(\mu - 1) \tag{9}$$

where β_c and Y_c are the values of β and Y at the critical point ($\mu = 1$).

For each model the monthly mean values of Y and E_e/A_e from the control runs were fitted to equation 9 and 8 respectively using a least squares regression. For Amazonia and the Sahel all 12 months were utilised in the fitting exercise, but for the Southern European region only the months from April to September were used, to avoid periods when the available energy is so small that β is ill-defined. This procedure provides an estimate of the characteristics of each LSS in terms of β_c, Y_c, β' and Y'. Values for Amazonia, the Sahel and Southern Europe are given in tables 3, 4 and 5.

a Estimating the surface hydrology of the control climate

In this section we test the characterisation of each LSS by attempting to predict its long-term mean soil moisture status and annual mean evaporation using information about the $1\times CO_2$ control climates. On the multi-annual timescale changes in soil moisture storage are negligible, so precipitation balances evapotranspiration and runoff:

$$E_e + Y = P_e \tag{10}$$

where P_e is the throughfall precipitation (i.e. precipitation minus interception). Substituting in equation 2, 8 and 9 gives:

$$A_e\{\beta_c + \beta'(\mu - 1)\} + Y' + Y'(\mu - 1) = P_e \tag{11}$$

Thus our simple model predicts a long-term annual mean value of μ in terms of the control climate (P_e and A_e) and the surface characteristics (β_c, β', Y_c and Y'):

$$\mu = \frac{P_e + A_e\{\beta' - \beta_c\} + Y' - Y_c}{A_e\beta' + Y'} \tag{12}$$

Substituting this form for μ into equations 2 and 8 also yields an expression for the annual mean evaporation:

$$E_e = \frac{\beta_c Y' - \beta' Y_c}{A_e\beta' + Y'} \tag{13}$$

Figure 2 compares the values of μ and E predicted by equations 12 and 13 to the long-term means taken from each of the $1\times CO_2$ GCM runs. The simple linear characterisation of each LSS is clearly able to capture the large variation in moisture stress between the models for each of the three regions.

Note here that the models which are moisture stressed ($\mu < 1$) tend to have large values of Y_c (see tables 3, 4 and 5). For example, in Amazonia (figure 1a), negligible runoff occurs at the critical point in the Ha and Hb models, and these models are not moisture limited, whilst Ua, Ub, La and Lb all have significant runoff below the critical point, and these models are confined to the moisture limited regime. Insight into this can be gained by examining the conditions required for evaporation to be moisture unlimited. From equation 11, $\mu \geq 1$, if:

$$\chi \leq 1 - \phi \tag{14}$$

where we have defined two new dimensionless parameters:

$$\phi = \frac{\beta_c A_e}{P_e} \tag{15}$$

$$\chi = \frac{Y_c}{P_e} \tag{16}$$

The parameter, ϕ, is akin to Budyko's aridity index as described by Koster and Suarez (accepted for publication), whilst χ represents the runoff fraction when $\mu = 1$. Values of both parameters are given in tables 3, 4 and 5. There is a fairly consistent trend in the LSSs over all three regions, with Ha, Hb and then Ca being the least stressed (see figure 2), regardless of the ordering of ϕ between the LSSs.

b Estimating the hydrological response to climate change

Having demonstrated that the simple linear characterisation can capture the annual mean surface hydrology predicted by each LSS, here we extend the method to analyse the changes in surface hydrology on doubling CO_2. Specifically, we consider the changes in annual mean soil moisture and evaporation arising from a prescribed climate change, as given by the changes in throughfall precipitation, ΔP_e, and effective available energy, ΔA_e. The perturbation equation for the annual mean hydrological balance (equation 12) is:

$$\Delta A_e\{\beta_c + \beta'(\mu - 1)\} + \Delta\mu\{A_e\beta' + Y'\} = \Delta P_e \tag{17}$$

where $\Delta\mu$ is the change in the scaled annual mean soil moisture resulting from the prescribed climate perturbation (ΔP_e and ΔA_e). The expression for $\Delta\mu$ can be simplified using equation 8:

$$\Delta\mu = \frac{1}{Y'\{1+\zeta\}}\Delta P_e - \frac{\beta}{Y'\{1+\zeta\}}\Delta A_e \tag{18}$$

Here, a further dimensionless parameter, ζ has been introduced, which represents the ratio of the sensitivities of evaporation and runoff to soil moisture:

$$\zeta = \frac{\beta' A_e}{Y'} \tag{19}$$

The corresponding perturbation to the evaporation is derived from equations 2 and 8:

$$\Delta E_e = \beta\Delta A_e + \beta' A_e \Delta\mu \tag{20}$$

The soil moisture perturbation $\Delta\mu$ can be eliminated using equation 18, to give an expression for the change in evaporation resulting from ΔA_e and ΔP_e:

$$\Delta E_e = \frac{\zeta}{1+\zeta}\Delta P_e + \frac{\beta}{1+\zeta}\Delta A_e \tag{21}$$

This equation has been written in the form of the "chain-rule" to allow easy identification of the coefficients representing the sensitivity of evaporation to precipitation and available energy respectively:

$$\begin{aligned} \frac{\partial E_e}{\partial P_e} &= \frac{\zeta}{1+\zeta} \\ \frac{\partial E_e}{\partial A_e} &= \frac{\beta}{1+\zeta} \end{aligned} \tag{22}$$

Values for these coefficients, as diagnosed from the $1\times CO_2$ control climates, are given in tables 3, 4 and 5.

4 Climate Change Prediction

This characterisation is now applied to the three regions to aid the understanding of how each LSS responds to the simulated climate change.

a Amazonia

The annual mean control climates are paired according to their host GCM (figure 3a) with the CNRM and Hadley Centre GCMs producing much more rainfall than the LMD and University of Reading models. The Hadley Centre models are nearest to the observations (New *et al* (1997)).

The corresponding evaporation spread is dependent on both the atmospheric conditions and the LSS characteristics. However, the large discrepancy in runoff characteristics, particularly Y_c, is a primary factor in governing the extent of the moisture stress and therefore the evapotranspiration. This can be demonstrated by considering the minimum throughfall that would be required for Ha and La to be unstressed (see equation 14). Given an available energy of 5 mm day^{-1}, the throughfall required would be 3.4 and 7.1 mm day^{-1} for Ha and Lb respectively, a range which encompasses all of the GCM simulated annual precipitation values for this region. Thus, here at least, differences between the simulated soil moisture states are as dependent on variations amongst the LSSs as on variations in the simulated precipitation. This has implications for the response of the LSSs to a change in climate forcing.

Unlike the control simulations, the climate forcing and surface response anomalies are no longer clearly paired according to GCM (figure 3c). In all the simulated climate change experiments the annual mean precipitation is reduced and the available energy is increased. Inspite of this, two of the LSSs (Ha and Ca) produce an increase in evaporation, and the other six show a decrease (figure 3d). This disparity may be understood in terms of the linear characterisation, which successfully reproduces all the LSSs responses that do not include the effect of atmospheric CO_2 on stomatal closure (i.e. not Hb and Cb) (see figures 3e and 3f). (A good prediction is not expected for Hb and Cb because CO_2 dependent stomatal closure leads to reduced values of β_c and β' in the $2\times CO_2$ simulations. They therefore tend to conserve more soil moisture than is predicted. An estimate of the effect of enhanced stomatal closure can be made by extrapolating to the y=x line).

Although the linear methodology qualitatively reproduces the LSSs response it tends to underestimate the evapotranspiration and soil moisture changes in this region. This can be explained in part by the fact that reducing the soil moisture content makes the fitted β gradient larger, and the runoff gradient smaller in the $2\times CO_2$ simulations. Hence the fitted estimates of $(Y')^{-1}$ and β' from the $2\times CO_2$ runs are larger (not shown). Since only the fits from the $1\times CO_2$ simulations are used to estimate ζ, this results in an underprediction of the change in evaporation and soil moisture. Conversely an increase in soil moisture would imply an overestimate of these changes.

The LSSs responses vary from being almost completely dominated by energy availability to mainly dependent on throughfall supply (see figure 3g). Ca, Cb, Ha and Hb all have low critical runoff values, which results in them being beyond the active soil moisture region ($\mu > 1$) and therefore having small ζ values. Their relative positions can be explained in terms of how unstressed they are and therefore

how small β' is, which is again ultimately dependent on Y_c. In the absence of any other factors Ca, Cb, Ha and Hb should be primarily affected by the increase in available energy, not throughfall reduction. This results in an evaporation increase for Ca and Ha. Stomatal closure in the $2\times CO_2$ Cb and Hb simulations results in a net reduction in evaporation rate.

The remaining models have higher critical runoff values implying larger ζ values ($\beta' \sim \beta_c$) and more water stress. Generally the larger the value of ζ, the more sensitive the LSS is to throughfall and the less sensitive it is to available energy (see equation 18).

The scatter between the University of Reading and LMD model sensitivities is predominantly due to the differing available energies in the control simulations and the large β_c value in the bucket model, Lb. The latter is presumably related to the fact that Lb has no stomatal resistance. It has a value which is significantly greater than 1, which is likely to be due to a combination of factors, including possible sensible heat advection and the potential break down of the linear approximation when extrapolating from relatively small values of μ to the critical point.

Overall in this region, the less moisture stressed the LSS, the smaller the sensitivity of evapotranspiration to throughfall and the greater the sensitivity to available energy. The LSS scaled soil moisture sensitivity to both throughfall and energy availability also increases with decreasing stress.

The LSS characteristics and climate forcing changes have to be considered together when analysing the differences in the predicted evaporation change. The University of Reading schemes have practically identical characteristics and therefore very similar sensitivities to climate forcings. However, the rooting depth does affect the hydrological inertia of the LSS, and therefore its seasonal behaviour and subsequent interaction with the atmosphere, resulting in very different annual mean precipitation and evaporation anomalies. The combined effect of the relatively high throughfall sensitivity and strong atmospheric changes result in Ub having the largest absolute changes in evaporation (ignoring differences in interception parameterisation). Even though Lb is the most sensitive to throughfall, it experiences little change in this forcing term, resulting in a neglible change in evaporation.

b The Sahel

There is a large variation in the annual mean precipitation and an even greater spread in the net radiation in the control climate runs (figure 4a), with a smaller scatter in evaporation and runoff (figure 4b). All the models except Ca and Cb significantly overestimate annual mean precipitation. With the exception of the LMD models, the LSSs tend to be paired according to the GCM.

All the models apart from Hb show a reduction in annual mean precipitation (figure 4c). However some of these values are extremely small. There is a small increase in available energy in all cases. Only Ha simulates an increase in evapotranspiration (figure 4d). The change in runoff is more scattered. Generally the anomalies are less paired according to GCM than in the control state.

The evaporation and scaled soil moisture changes are well reproduced, with the exception of La and CNRM, which have poor runoff fits, and Hb (see figures 4e and 4f). Hb includes significant CO_2-induced stomatal closure, explaining why the linear characterisation overestimates evaporation and soil moisture change. In general we can still use the linear characterisation to help explain some of the main differences in model behaviour.

There is a significant scatter in the LSS sensitivity, varying from being entirely throughfall dependent (Lb) to being sensitive to both forcing parameters (Ua and Ub) (see figure 4g). All the models have μ values around or less than 1, leading to non-zero β' values. The differences in ζ and therefore water and energy sensitivity between Ha, Hb, Ca, Cb, Ua and Ub are consequently mainly due to increasing Y' (and therefore Y_c). The large amount of available energy in the La and Lb control simulations is also significant. The primary difference in the La and Lb sensitivities is due to the latter having no stomatal resistance.

When analysing the absolute differences in evaporation and precipitation, the spread in LSS sensitivities must be viewed in conjunction with the climate forcing changes. As in Amazonia there is little difference between the University of Reading models' LSS sensitivities. The differences in the absolute changes in precipitation and evaporation are relatively small, however they could still be partially due to inertial effects (as in Amazonia). Even though the changes in evaporation in the University of Reading models are very close to those of the other models, their precipitation reduction is much larger implying that the atmospheric forcing is significantly different for these models.

The CNRM models show very similar changes in precipitation and evaporation because in these simulations bare soil evaporation dominates over this region, and therefore the stomatal closure in Cb

has a negligible influence.

c Southern Europe

There is a large disparity in the control climates (figure 5a), with the LMD models strongly overestimating precipitation and simulating much more net radiation. There is also a large amount of scatter in evaporation (figure 5b). The Hadley Centre and University of Reading models are paired together in both forcing and surface fields (Ca and Cb are identical by definition).

There is no consensus even in the predicted sign of the annual mean change in rainfall (figure 5c). The Hadley Centre and LMD models predict a reduction in precipitation and the CNRM and University of Reading models an increase, albeit with a smaller magnitude. There is a similar split with the evaporation changes. All the models except the LMD models show an increase in available energy. The pairing is weaker in the anomalies than the control simulations.

Ignoring Hb, where stomatal dependence of atmospheric CO_2 has a significant impact, the technique predicts the changes reasonably well (see figures 5e and 5f). The annual mean change in soil moisture is basically correctly ordered, although the sign of the change is incorrect for some of the models which have a relatively small soil moisture change. Overall the linear characterisation sensitivities may be applied to help understand the spread in the anomalies.

The aridity index is relatively high, making all the models moisture stressed for at least some of the year. Variation in ζ is therefore mainly due to Y' and by implication Y_c. The large amount of energy available to La and Lb increases ζ further in these cases.

Here again, the bare soil evaporation is a significant portion of the total evaporation in the CNRM models and therefore the effect of stomatal closure is relatively small.

5 Isolating the causes of the different hydrological sensitivities

The results presented above in section 4 demonstrate that the simple linear characterisation of the LSSs is able to reproduce many of the features of the GCM-generated changes in soil moisture and evaporation. In general the simple linear model can duplicate the order of the changes simulated in each GCM-LSS pair and in most cases fits the actual changes from the GCM well.

The linear perturbation equations (18 and 21) show how the different hydrological responses to climate change can be understood in terms of differences in the GCM-generated climate change (i.e. differences in ΔP_e and ΔA_e), plus differences in the hydrological sensitivity coefficients such as those given in equation 22. The latter are explicitly dependent on both the control climate (through A_e), the control hydrology (through β) and the surface scheme (through β' and Y').

However, there are also implicit dependencies hidden in these sensitivity coefficients. Section 3 showed how the control hydrological state (as expressed by μ and E_e) is a function of the surface scheme and the control climate. Also, there is evidence from figure 1 that the different values of β' (and to a lesser extent Y') are as much a function of the hydrological regime as of the surface scheme per se.

In this section we set out to disentangle the effects of the LSS and the host GCM on the moisture stress in the control simulation, and on the evaporation sensitivity coefficients (equation 22). Such an analysis excludes feedbacks between the surface state and the climate, but otherwise should allow us to estimate the outcome of coupling a given LSS to a given GCM. In order to do this we consider a number of hypothetical LSSs and force them with a range of climates. We return to the underlying non-linear model as represented by equations 2, 4 and 5.

The climate forcing and LSS characteristics are isolated by using the parameters ϕ and χ as the control variables representing the climate and the LSS respectively. In terms of these parameters, the fraction of the throughfall which forms evapotranspiration (as given by equations 2 and 4) becomes:

$$\frac{E_e}{P_e} = \begin{cases} \phi\mu & \text{for } \chi > 1-\phi \\ \phi & \text{for } \chi \leq 1-\phi \end{cases} \tag{23}$$

where equation 14 has been used to distinguish between the moisture limited ($\mu < 1$) and the non-moisture limited regimes ($\mu \geq 1$). Similarly, the evaporation sensitivity coefficients given by equation

22 are also a function of ϕ, χ and μ only. The sensitivity of evapotranspiration with respect to throughfall becomes:

$$\frac{\partial E_e}{\partial P_e} = \begin{cases} \dfrac{\phi}{\phi + c\,\mu^{c-1}\,\chi} & \text{for } \chi > 1-\phi \\ 0 & \text{for } \chi \leq 1-\phi \end{cases} \tag{24}$$

and its sensitivity to effective available energy is:

$$\frac{\partial E_e}{\partial A_e} = \begin{cases} \dfrac{\beta_c\, c\,\mu^c\,\chi}{\phi + c\,\mu^{c-1}\,\chi} & \text{for } \chi > 1-\phi \\ \beta_c & \text{for } \chi \leq 1-\phi \end{cases} \tag{25}$$

Of course, the scaled soil moisture, μ, is itself a function of climate and the LSS, as discussed in section 3. The annual mean water balance (equation 10) provides algebraic equations for μ as a function of ϕ and χ. In the non-stressed regime ($\chi \leq 1-\phi$):

$$\chi\,\mu^c + \phi = 1 \tag{26}$$

so the scaled soil moisture is given by:

$$\mu = \left\{\frac{1-\phi}{\chi}\right\}^{1/c} \tag{27}$$

In the stressed regime ($\chi > 1-\phi$) μ satisfies a polynomial:

$$\chi\,\mu^c + \phi\,\mu - 1 = 0 \tag{28}$$

Estimates of the exponent c can be obtained from the previous linear characterisation by calculating the ratio Y'/Y_c. Typically the regional average Y versus μ curves yield values of c between 1 and 2 (not shown). For $c = 1$ the model reverts to a linear runoff versus μ curve which passes through the origin. The full solution for this special case is shown in table 6. The case $c = 2$ provides the simplest model which has non-linearity in both the β and runoff curves, and it should therefore provide some qualitative indication of the behaviour of the model for all powers greater than 1. For $c = 2$ equation 28 is a quadratic with a single physically meaningful root:

$$\mu = \frac{\phi}{2\chi}\left[\left\{1 + \frac{4\chi}{\phi^2}\right\}^{1/2} - 1\right] \tag{29}$$

The solutions for μ given by equations 27 and 29 can be substituted into equations 23, 24 and 25 to give forms for the annual mean evaporation and its sensitivity to climate change, which are dependent on χ and ϕ only. Figure 6 shows the behaviour predicted by this simple non-linear model as a function of the climate state, as defined by the aridity index ϕ, and the LSS, as defined by χ.

The two hydrological regimes are very evident. In the region of parameter space for which $\chi \leq 1-\phi$, μ is greater than 1 and evaporation is not moisture limited. The evaporation is insensitive to changes in soil moisture, but has a sensitivity to available energy given by β_c (set to 1 in figure 6). This regime therefore represents a point in the lower right corner of figure 6c. The GCM experiments which most clearly inhabit this part of the climate-LSS parameter space are the Hadley Centre runs (Ha and Hb) in Amazonia. The fact that Ha and Hb both have $\mu > 1$ in this region is consistent with our simple non-linear model, as are their small sensitivities to precipitation and their large sensitivities to available energy (see figure 3g). Likewise, the CNRM model has $\chi \approx 1-\phi$ and $\mu \approx 1$ in this region, and once again this model inhabits the lower right corner of the evaporation sensitivity plot.

Considering a typical tropical climate such as Amazonia ($P \sim 6$mm day^{-1}, $A \sim 4$mm day^{-1} and $\phi \sim 0.75$) increasing the critical runoff from 0 to 3mm day^{-1} (typical of the spread scene in the LSSs in this region) results in a change from complete dependency on available energy (1.0) to a roughly equal dependence on both forcing parameters of 0.5.

In the remainder of the parameter space $\chi > 1-\phi$ and evaporation is moisture stressed. In this regime, evaporation and soil moisture still decrease with increasing χ, but the sensitivity coefficients

show more complex behaviour. The sensitivities of evapotranspiration to precipitation and available energy are a strong function of ϕ. In a typical semi-arid region like the Sahel ($P \sim 1.5$mm day^{-1} and $A \sim 3$mm day^{-1}) $\phi \sim 2$. A spread of χ from roughly 0 to 2, which is equivalent to the variation in Y_c ($\sim 0 \rightarrow 3$mm day^{-1}), results in a reduction of throughfall sensitivity of about 50%.

In arid environments (for which $\phi > 1$), evapotranspiration is much more dependent on precipitation than available energy, and $\partial E_e / \partial P_e$ is itself a strongly decreasing function of χ. The opposite occurs in moist environments, where $\partial E_e / \partial A_e$ dominates but decreases rapidly with increasing χ.

Overall the sensitivity of scaled soil moisture to changes in both throughfall and available energy reduces with increasing critical runoff. The scaled sensitivity to throughfall becomes more important relative to available energy as the aridity is reduced.

6 Conclusions

We have analysed results from 8 climate change experiments which were carried out as part of an EU project on "Climate and Land Surface Processes". The simulations used 4 separate GCMs, and each of these included 2 distinct land surface schemes (LSSs). In the absence of a common coupling interface, such as that currently under development in PILPS phase 4 (Polcher *et al* (1998)), it was not feasible to use the same LSS in more than one GCM. Instead, the differences between the LSSs were chosen at the discretion of each participating group. This approach prevented the complete diagnosis of the impact of each LSS (including feedbacks), but guaranteed that a large range of parameterisations would be used.

In order to understand the role of the LSSs in the GCM simulations of climate and climate change, a simple characterisation has been developed based on a generic "bucket" model, in which each LSS is described by curves representing runoff (Y) and evaporative fraction (β) as a function of scaled rootzone soil moisture (μ). This characterisation has been applied to isolate the impact of LSS differences on the GCM predicted changes in surface hydrology, over three very different climatic regions (Amazonia, the Sahel and Southern Europe).

A linearisation of the bucket model was able to reproduce the very different soil moisture regimes experienced by each GCM-LSS pair. In each region, the range of simulated soil moistures was shown to be dependent on the variation between both the LSSs and the control climates. There is also likely to be a feedback between the two from moisture recycling. The most important LSS differences were summarised in terms of the runoff, Y_c, which occurs when evaporation is marginally moisture-limited (i.e. at the critical soil moisture). The higher this critical point runoff is, the more moisture stressed the model tends to be.

The variation in the LSS responses has been analysed by partitioning the behaviour into two parts; throughfall and available energy sensitivity. The magnitude of these terms is highly dependent on the control climate and the LSS, and on the interaction between the two. In very arid regions the LSSs are primarily dependent on throughfall changes, regardless of whether evaporation is moisture limited or not. The sensitivity decreases significantly with increased moisture stress, however. In moist climates, the models may range from mainly sensitive to available energy changes if they are unstressed, to predominantly sensitive to throughfall if moisture stressed.

Such a large spread was simulated over Amazonia. This explained why all the LSSs without CO_2-induced stomatal closure, except two, simulated a reduction in evaporation, even though they all had qualitatively similar forcing perturbations. The models singled out here tended not to be moisture limited and therefore more dependent on the energy increase rather than the rainfall reduction. Such gross variation in the land surface response can occur in any region which experience perturbations in the two surface drivers of opposite signs. In the other regions studied there was still a substantial scatter in the LSS sensitivities.

In some respects, the use of regional averages complicates the analysis, because the non-linear nature of the evaporative fraction and runoff curves makes them sensitive to soil moisture heterogeneity. However, the idealised, piecewise linear $\beta - \mu$ curve still appears to offer a valuable conceptual model, separating the moisture-limited and non-moisture-limited regimes clearly. Also, whilst soil moisture heterogeneity might be expected to enhance regional-scale runoff, differences amongst the LSS runoff characteristics are much larger than could be explained by different sub-regional soil moisture distributions. Instead, the different LSS runoff characteristics are probably indicative of assuming different parameters at the gridpoint scale.

For example, the LSS used in the Hadley Centre "b" experiment shares a similar soil model structure to that used in the University of Reading simulations. Both LSSs use Darcy's equation to simulate vertical flow between 4 soil layers and each describes the variation of soil water suction and hydraulic conductivity with soil moisture concentration according to Clapp and Hornberger (1978). Both schemes also have similar definitions of the wilting and critical soil moisture concentrations (defined as the soil moistures for which the suction equals -1.5 MPa and -0.0033 MPa respectively). The major differences are in the choice of extremely variable soil parameters such as the saturated soil water suction and the saturated hydraulic conductivity. The different values chosen yield values of Y_c of 1.3 and 0.014 mm day^{-1} respectively for Ua (Ub) and Hb respectively in Amazonia. Such a discrepancy partially explains the very different moisture regimes simulated in these experiments.

Overall, our analysis supports many of the conclusions of Koster and Milly (1997). We have found that differences amongst the GCM predictions of changes in surface hydrology are particularly sensitive to how the runoff is parameterised over the active soil moisture range. Variations in the runoff at the critical soil moisture point (below which evaporation is moisture-limited), account for much of the spread in the GCM predictions of hydrological change. Reducing the uncertainties in these predictions will require improved treatments of runoff appropriate for the GCM spatial resolution, rather than further sophistication in the treatment of evapotranspiration at the point scale.

Acknowledgments

This study was carried out as part of the EU Climate and Environment Programme under contract ENV4-CT95-0112-PL950189. Peter Cox was also supported by the UK DETR Climate Prediction Programme under contract PECD 7/12/37.

References

Clapp, R., and G. Hornberger, 1978: Empirical equations for some soil hydraulic properties. *Water Resources Research*, **14**, 601–604.

Cox, P. M., R. A. Betts, C. B. Bunton, R. L. H. Essery, P. R. Rowntree, and J. Smith, 1999: The impact of new land surface physics on the GCM sensitivity of climate and climate sensitivity. *Climate Dynamics*, **12**.

Douville, H., S. Planton, J.-F. Royer, D. B. Stevenson, S. Tyteca, L. Kergoat, S. Lafont, and R. A. Betts, submitted: Relevance of the vegetation feedbacks in double-CO2 timeslice experiments. *Journal of Geophysical Research.*

Ducoudre, N., K. Laval, and A. Perrier, 1993: Sechiba, a new set of parameterisations of the hydrological exhanges at the land/atmosphere interface with the lmd atmospheric general circulation model. *Journal of Climate*, **6**(2), 248–273.

Entekhabi, D., and P. Eagleson, 1989: Land surface hydrology parameterization for atmospheric general circulation models including subgrid spatial variability. *Journal of Climate*, **2**, 816–831.

Gates, W., 1992: The atmospheric model intercomparison project. *Bulletin of the American Meteorological Society*, **73**, 1962–1970.

Gregory, J. M., J. F. B. Mitchell, and A. J. Brady, 1997: Summer drought in northern mid-latitudes in a time-dependent CO_2 climate experiment. *J. Climate*, **10**, 662–686.

Henderson-Sellers, A., K. McGuffie, and A. Pitman, 1996: The project for intercomparison of land-surface parametrization schemes (PILPS): 1992-1995. *Climate Dynamics*, **12**(12), 849–859.

Houghton, J. T., L. G. M. Filho, B. A. Callander, N. Harris, A. Kattenberg, and K. M. (eds), 1995: *Climate Change 1995.* Cambridge University Press.

Koster, R. D., and P. C. D. Milly, 1997: The interplay between transpiration and runoff formulations in land surface schemes used with atmospheric models. *Journal of Climate*, **10**(7), 1578–1591.

Koster, R., and M. Suarez, accepted for publication: A simple framework for examining the interannual variability of land surface moisture fluxes. *Journal of Climate.*

Manabe, S., 1969: Climate and ocean circulation, 1. The atmospheric circulation and the hydrology of the earth's surface. *Monthly Weather Review*, **97**, 739–774.

Mitchell, J. F. B., T. C. Johns, J. M. Gregory, and S. F. B. Tett, 1995: Climate response to increasing levels of greenhouse gases and sulphate aerosols. *Nature*, **376**, 501–504.

New, M., M. Hulme, and P. Jones, 1997. Representing twentieth century space-time climate variability. I: Development of a 1961-1990 mean monthly terrestrial climatology. Submitted to Journal of Climate.

Noilhan, J., and S. Planton, 1989: A simple parameterisation of the land surface processes for meteorological models. *Monthly Weather Review*, **117**(3), 536–549.

Polcher, J., B. McAvaney, P.Viterbo, M.-A. Gaertner, A. Hahmann, J.-F. Mahfouf, J. Noilhan, T. Phillips, A. Pitman, C. Schlosser, J.-P. Schulz, B. Timbal, D. Verseghy, and Y. Xue, 1998: A proposal for a general interface between land surface schemes and general circulation models. *Global and Planetary Change*, **19**, 261–276.

Viterbo, P., and C. Beljaars, 1995: An improved land surface parameterisation scheme in the ecmwf model and its validation. *Journal of Climate*, **8**, 2716–2748.

Warrilow, D. A., and E. Buckley, 1989: The impact of land surface processes on the moisture budget of a climate model. *Annales Geophysicae*, **7**, 439–450.

Meteo-France (CNRM)	Ca Cb	ISBA scheme (Noilhan and Planton (1989)) +reduced stomatal conductance Douville *et al* (submitted)
Hadley Centre (HC)	Ha Hb	Old land surface scheme (Warrilow and Buckley (1989)) MOSES (Cox *et al* (1999))
Laboratoire de Meteorologie Dynamique (LMD)	La Lb	SECHIBA scheme (Ducoudre *et al* (1993)) Simple bucket (Manabe (1969))
University of Reading (UR)	Ua Ub	ECMWF scheme (Viterbo and Beljaars (1995)) half rooting depth

Table 1: The land surface schemes used in the time-slice experiments

Amazonia	70.1W to 49.9W and 15.1S to 0.1N
Sahel	15.1W to 25.1E and 9.9N to 18.1N
Southern Europe	10.1W to 25.1E and 34.9N to 47.0N

Table 2: The regions highlighted in this paper

	Ca	Cb	Ha	Hb	La	Lb	Ua	Ub
β_c	0.76	0.76	0.68	0.68	0.87	1.94	0.81	0.74
β'	0.42 (0.08)	0.42 (0.08)	0.03 (0.04)	0.16 (0.05)	0.69 (0.04)	1.72 (0.05)	0.77 (0.08)	0.62 (0.08)
Y_c (mm day^{-1})	2.53	2.53	-0.56	0.6	2.79	4.28	2.81	2.75
Y' (mm day^{-1})	4.13 (0.90)	4.13 (0.90)	1.51 (0.45)	3.82 (0.54)	2.78 (0.56)	4.33 (0.27)	3.72 (0.38)	3.25 (0.40)
ϕ	0.45	0.45	0.58	0.56	1.53	2.92	1.19	1.02
χ	0.56	0.56	-0.13	0.14	1.15	1.15	1.40	1.31
ζ	0.27	0.27	0.07	0.16	1.06	2.23	0.61	0.55
$\partial E_e/\partial P_e$	0.21	0.21	0.07	0.13	0.51	0.67	0.38	0.36
$\partial E_e/\partial A_e$	0.53	0.53	0.67	0.65	0.18	0.17	0.23	0.25

Table 3: Bucket model fitting parameters (β_c, β', Y_c, Y'), aridity index (ϕ), runoff fraction at the critical soil moisture (χ), ratio of the sensitivities of evaporation and runoff to soil moisture (ζ), and estimated sensitivities of evaporation to throughfall and effective available energy ($\partial E_e/\partial P_e$ and $\partial E_e/\partial A_e$); for the Amazonian region. Values in brackets refer to the root mean square error.

	Ca	Cb	Ha	Hb	La	Lb	Ua	Ub
β_c	0.94	0.94	0.41	0.45	0.65	2.3	0.82	0.81
β'	0.52 (0.10)	0.52 (0.10)	0.17 (0.07)	0.33 (0.07)	0.71 (0.02)	2.14 (0.08)	0.69 (0.11)	0.63 (0.11)
Y_c (mm day^{-1})	1.15	1.15	0.38	0.55	1.99	1.87	3.19	3.32
Y' (mm day^{-1})	1.00 (0.25)	1.00 (0.25)	0.39 (0.16)	0.90 (0.23)	2.77 (0.31)	1.92 (0.10)	4.37 (0.43)	3.94 (0.46)
ϕ	1.68	1.68	0.80	0.84	2.16	4.06	0.99	1.01
χ	0.87	0.87	0.22	0.30	1.68	0.78	1.62	1.76
ζ	1.24	1.24	1.44	1.23	1.01	5.34	0.37	0.38
$\partial E_e/\partial P_e$	0.55	0.55	0.59	0.55	0.50	0.84	0.27	0.27
$\partial E_e/\partial A_e$	0.21	0.21	0.17	0.18	0.11	0.07	0.32	0.30

Table 4: As table 3 but for the Sahelian region.

	Ca	Cb	Ha	Hb	La	Lb	Ua	Ub
β_c	1.16	1.16	0.37	0.51	0.43	1.02	0.75	0.91
β'	0.57 (0.04)	0.57 (0.04)	0.24 (0.05)	0.30 (0.04)	0.21 (0.07)	0.75 (0.03)	0.47 (0.04)	0.66 (0.04)
Y_c	0.97	0.97	0.42	0.54	1.96	2.39	1.81	2.00
Y' (mm day^{-1})	0.74 (0.14)	0.74 (0.14)	0.28 (0.18)	0.55 (0.10)	2.52 (0.45)	2.54 (0.31)	1.99 (0.13)	2.23 (0.14)
ϕ	2.04	2.04	0.62	0.80	0.71	1.08	0.80	0.90
χ	1.07	1.07	0.31	0.37	0.25	0.27	0.47	0.53
ζ	1.23	1.23	1.94	1.23	0.24	1.16	0.40	0.48
$\partial E_e/\partial P_e$	0.55	0.55	0.67	0.55	0.19	0.54	0.28	0.33
$\partial E_e/\partial A_e$	0.17	0.17	0.10	0.18	0.27	0.24	0.40	0.37

Table 5: As table 3 but the Southern European region.

	$\chi > 1-\phi$	$\chi \leq 1-\phi$
μ	$\frac{1}{\phi+\chi}$	$\frac{1-\phi}{\chi}$
$\frac{E_e}{P_e}$	$\frac{\phi}{\phi+\chi}$	ϕ
$\frac{\partial E_e}{\partial P_e}$	$\frac{\phi}{\phi+\chi}$	0
$\frac{\partial E_e}{\partial A_e}$	$\frac{\beta_c \chi}{\{\phi+\chi\}^2}$	β_c
$P_e \frac{\partial \mu}{\partial P_e}$	$\frac{1}{\phi+\chi}$	$\frac{1}{\chi}$
$A_e \frac{\partial \mu}{\partial A_e}$	$-\frac{\phi}{\{\phi+\chi\}^2}$	$-\frac{\phi}{\chi}$

Table 6: Scaled soil moisture and evapotranspiration, and related sensitivity coefficients as calculated from the generic non-linear model with $c = 1$.

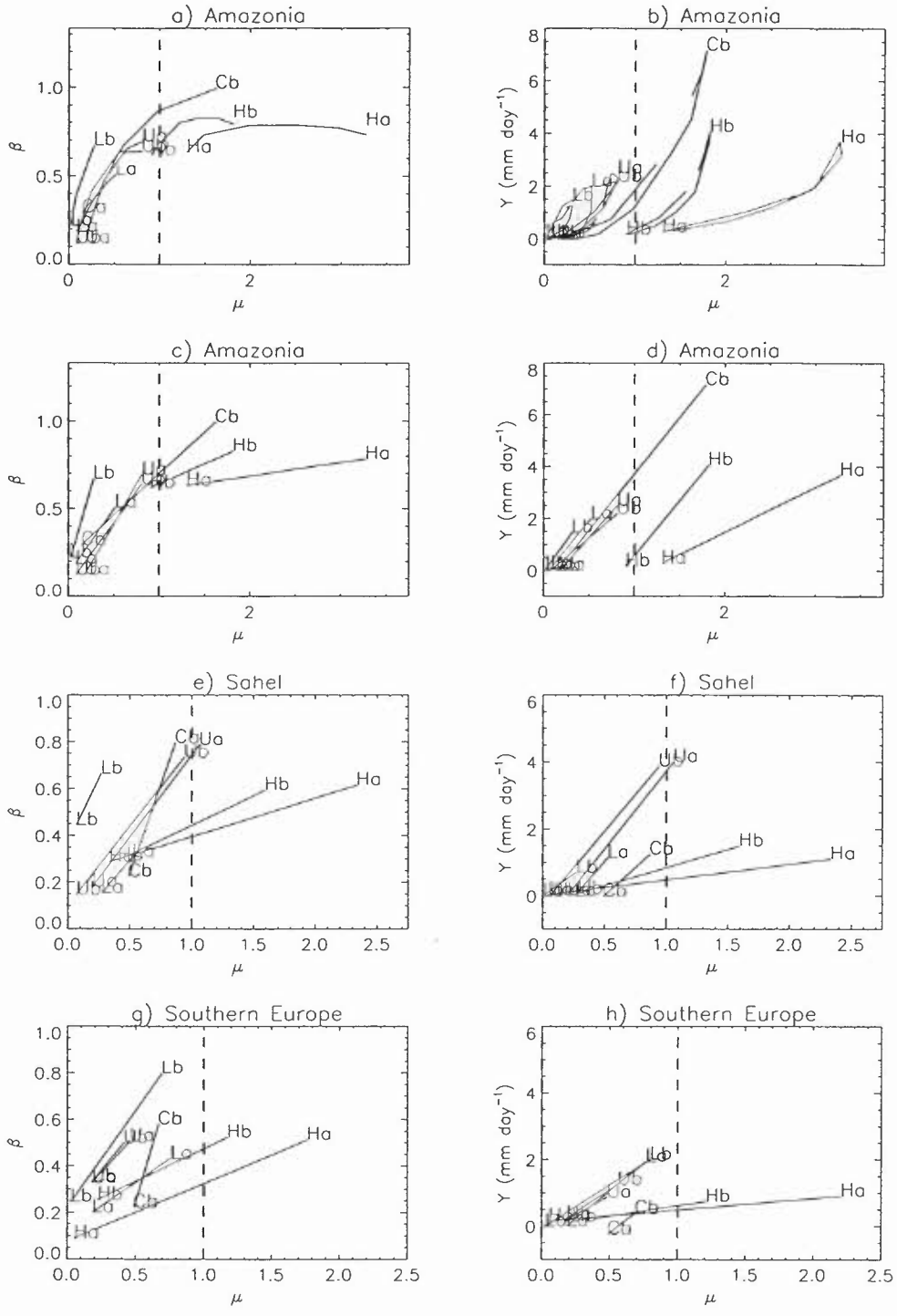

Figure 1: The dependence of runoff and evaporative fraction on scaled soil moisture. Plots (a) and (b) correspond to the raw monthly mean GCM data for Amazonia, whilst the other plots are linear model fits to Amazonia, Sahel and Southern Europe

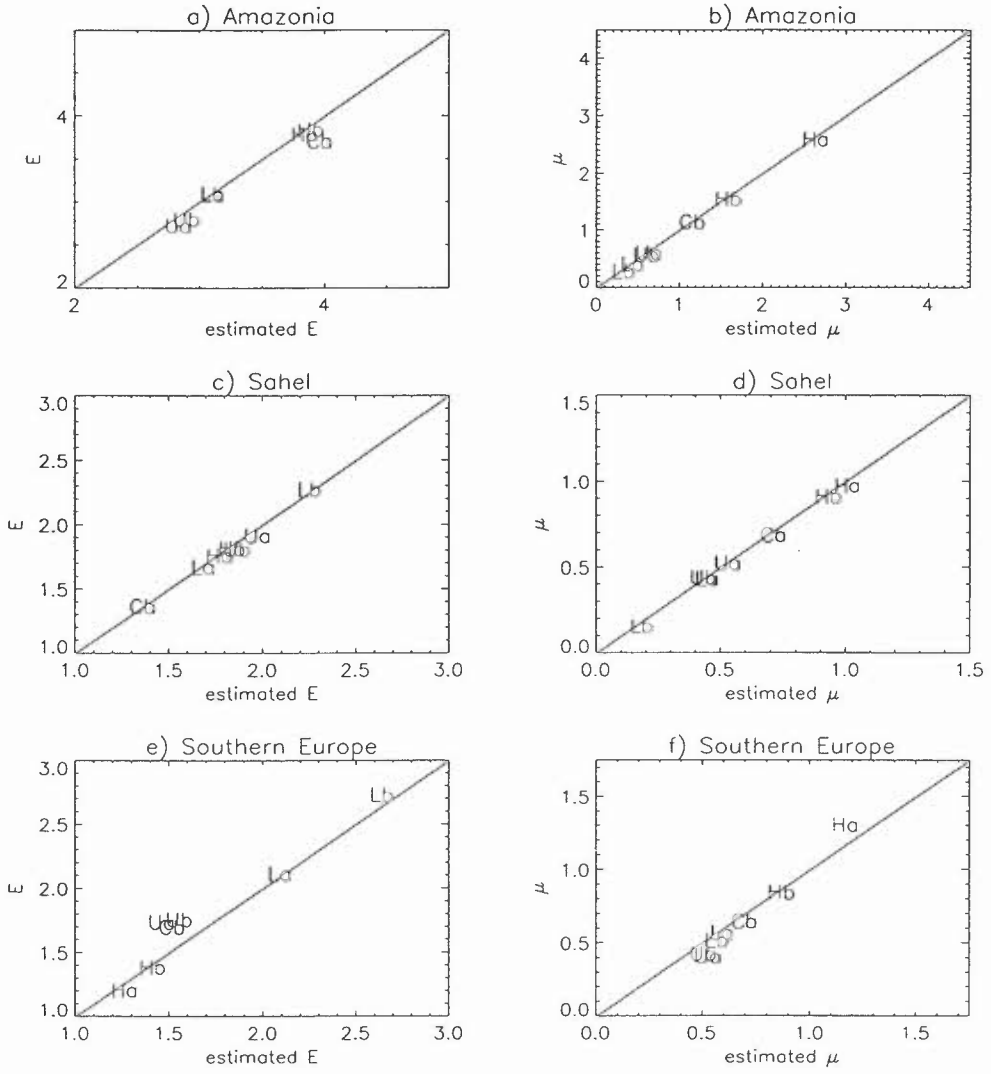

Figure 2: GCM annual mean evaporation (E) and scaled soil moisture (μ) versus estimates from the linear LSS characterisation for Amazonia, the Sahel and Southern Europe.

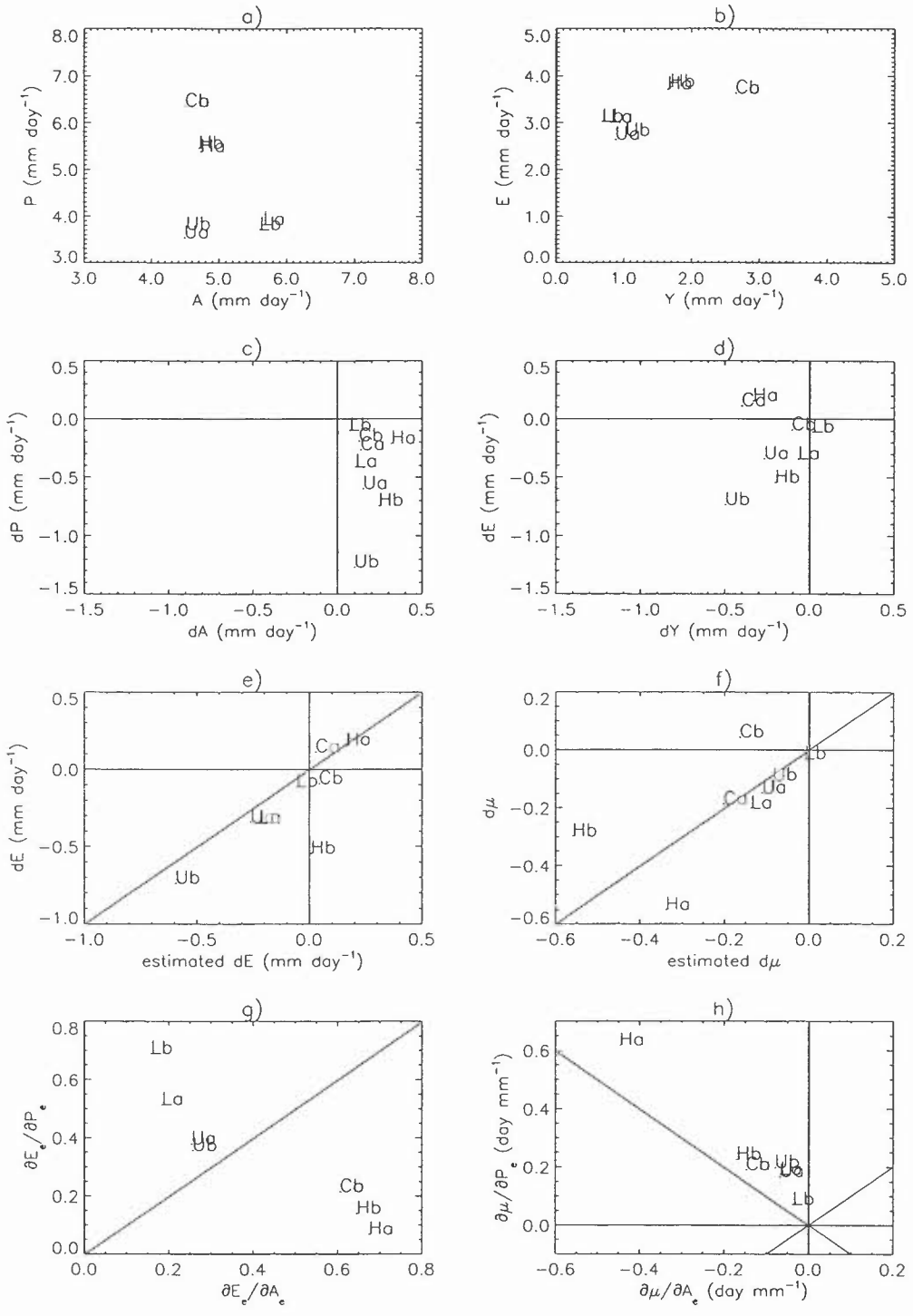

Figure 3: GCM predictions and the linear LSS characterisations for Amazonia. (a) GCM annual mean climate; (b) GCM annual mean hydrological fluxes; (c) GCM predicted climate change; (d) GCM predicted hydrological change; (e) GCM evaporation change versus the estimate from the linear characterisation; (f) GCM soil moisture change versus the estimate from the linear characterisation; (g) Estimated evaporation sensitivity coefficients; (h) Estimated soil moisture sensitivity coefficients. (The observed annual mean precipitation from New *et al* (1997) is 5.8 mm day^{-1}).

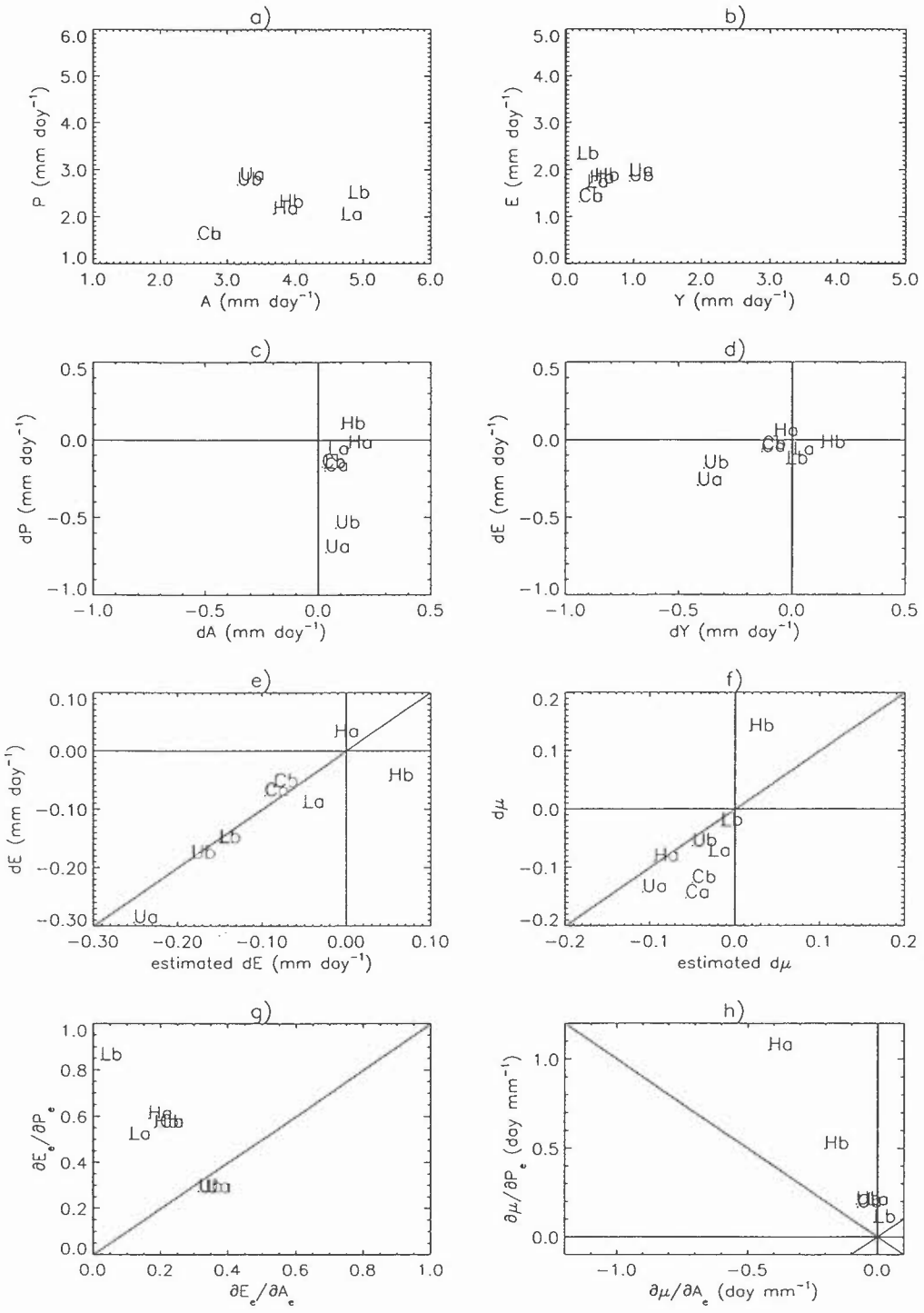

Figure 4: As for figure 3 but for the Sahel. (The observed annual mean precipitation from New *et al* (1997) is 1.4 mm day^{-1}).

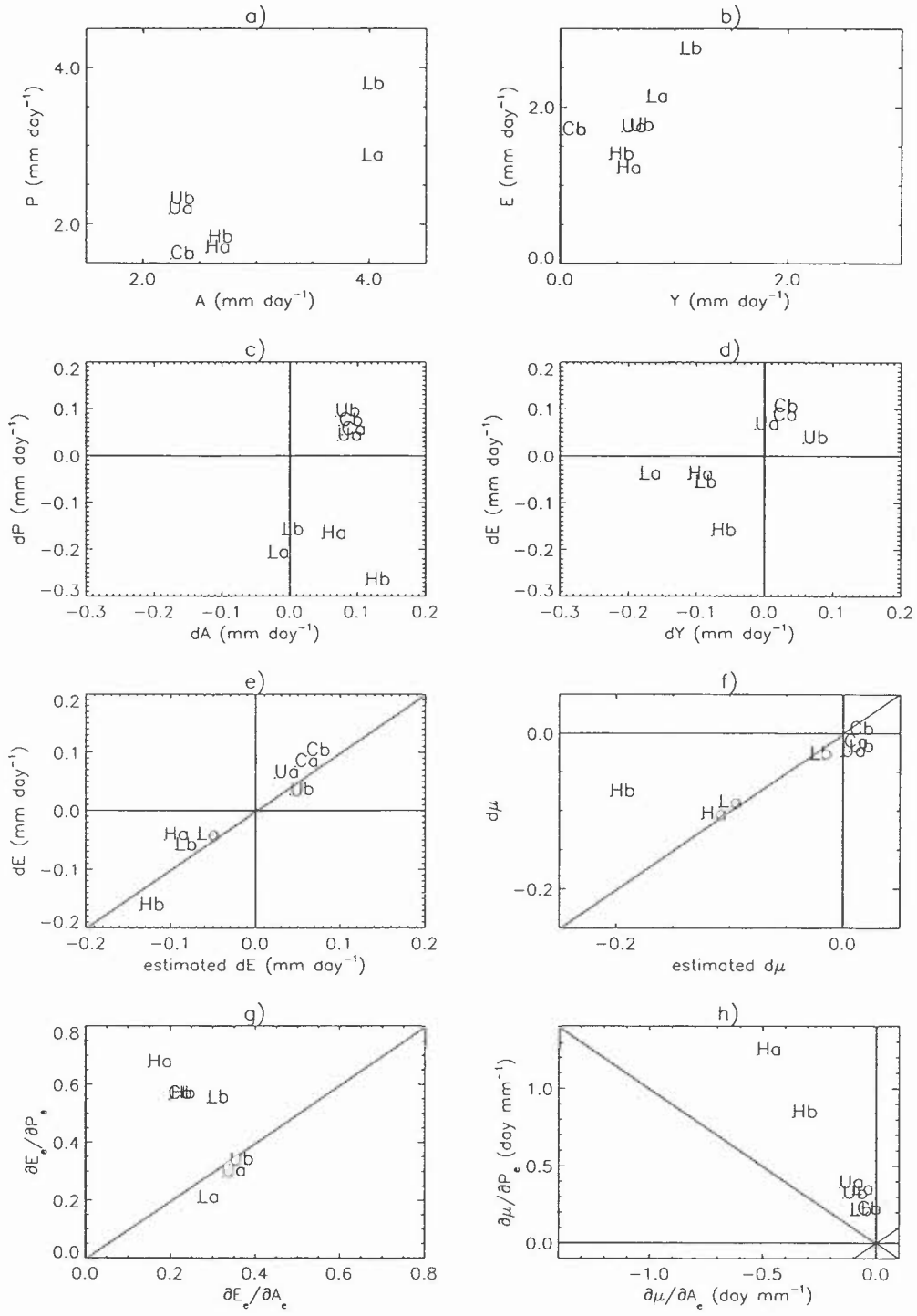

Figure 5: As for figure 3 but for Southern Europe. (The observed annual mean precipitation from New *et al* (1997) is 2.4 mm day^{-1}).

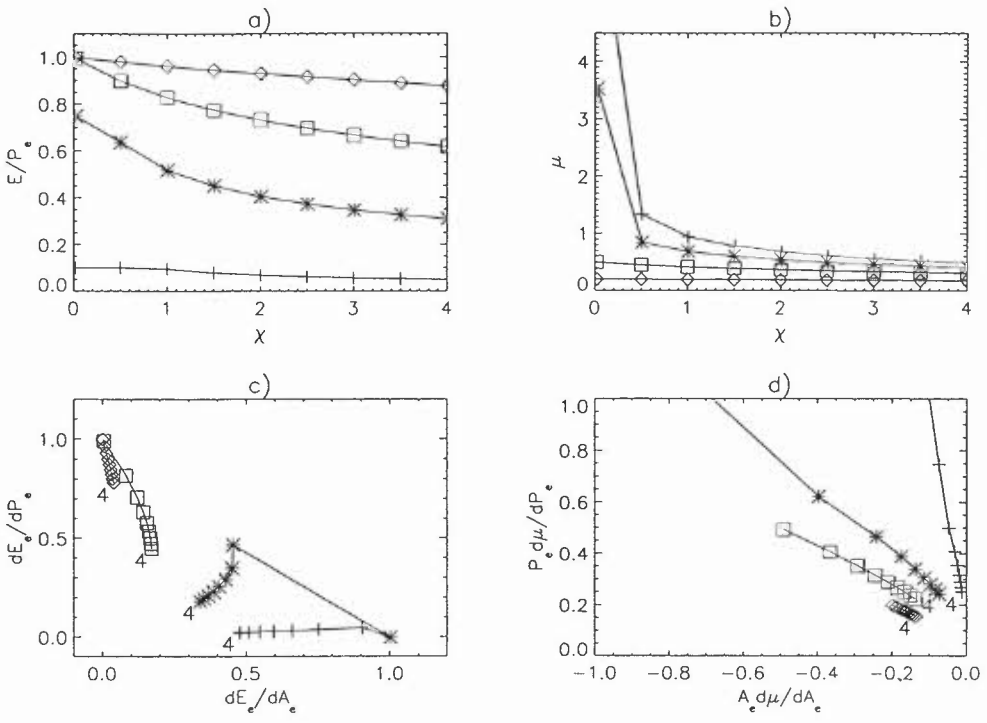

Figure 6: (a) Scaled evaporation; (b) scaled soil moisture; (c) evaporation sensitivity coefficients and (d) soil moisture sensitivity coefficients, from the non-linear bucket model with $c = 2$. (Crosses, stars, squares, and diamonds correspond to ϕ=0.1, 0.75, 2.0 and 5.0 respectively. χ=4 is marked in figures (c) and (d)).